High-Performance $Na_{3.5}Fe_{0.5}V_{1.5}(PO_4)_3$ Cathodes Enabled by Phase Control and CQD-Containing Carbon Coating

Haoyu Guonie, [a] *Changwei Shi* [b] *Changlian Chen,* [b] *Chaoqun Shang,* [a] *Pu Hu* [a*]

[a.] *State Key Laboratory of Green and Efficient Development of Phosphorus Resources, Hubei Key Laboratory of Plasma Chemistry and Advanced Materials, School of Materials Science and Engineering, Wuhan Institute of Technology, Wuhan, 430205, China.*

[b.] *School of Chemical Engineering & Pharmacy, Wuhan Institute of Technology, Wuhan, 430205, China*

Corresponding author：hupu@wit.edu.cn (P. Hu)

Experimental Section:

Material synthesis

All chemicals were of analytical grade and used as received without further purification. $Na_{3+x}Fe_xV_{2-x}(PO_4)_3$ materials (denoted as NF_xVP, where x = 0, 0.3, 0.5, 0.7, 1) were prepared via a sand-milling-assisted spray-drying method followed by thermal treatment under an inert atmosphere. Stoichiometric amounts of Na_2HPO_4, NaH_2PO_4, V_2O_5, $FeC_2O_4·2H_2O$, and $C_6H_8O_7·H_2O$ (citric acid monohydrate) corresponding to $Na_{3+x}Fe_xV_{2-x}(PO_4)_3$/C ($NF_xVP$, x = 0, 0.3, 0.5, 0.7, 1) were mixed with 120 mL deionized water in a milling jar. The slurry was homogenized by sand-milling (2000 rpm, 2 h). Subsequently, the mixture was spray-dried at 180°C to obtain yellow

precursor powder. This precursor was annealed under argon atmosphere with temperature programming: 400°C (4 h) and 750°C (15 h) at 5°C min^{-1} ramp rate. The final products were denoted as NF_xVP-CA. For comparison, NF_xVP was synthesized identically except with $C_6H_{12}O_6 \cdot H_2O$ (glucose monohydrate) as carbon source, labeled NF_xVP-Glc. Kilogram-scale synthesis of $NF_{0.5}$VP-CA was performed using a proportionally scaled-up process with industrial-grade equipment to ensure reaction homogeneity and efficiency. Specifically, stoichiometric amounts of raw materials were accurately weighed: Na_2HPO_4 1.065 kg, NaH_2PO_4 4.500 kg, V_2O_5 2.046 kg, $FeC_2O_4 \cdot 2H_2O$ 1.350 kg, and $C_6H_8O_7 \cdot H_2O$ 2.112 kg. These were dispersed in deionized water to prepare a slurry with a solid content of 40%, which was subsequently transferred into a 10 L industrial horizontal sand mill.

Material characterization

The crystal structure of the samples was characterized using X-ray diffraction (XRD, D8 ADVANCE, Bruker AG, Germany). The properties of the carbon layer of each sample were analyzed by Raman spectrometer (DXR Raman microscope, Semmerfeld, USA). The surface morphology was examined using a scanning electron microscope (SEM, SU-3500, Hitachi Limited, Japan) equipped with an energy dispersive spectrometer (EDS). Microscopic images of the samples were obtained via high-resolution transmission electron microscopy (HR-TEM, JEOL-ARM200F, Japan). X-ray photoelectron spectroscopy (XPS, ESCALAB Xi+, Semmerfeld, USA) was utilized to determine the elemental valence. The specific surface area and pore size distribution of each sample were measured using the N_2 adsorption/desorption method with powder

process equipment (Anton paar IQ, Anton Paar China).

Electrode fabrication and electrochemical measurement

The electrochemical performance of the electrode was evaluated using a CR2032 button cell. To fabricate the cathode electrode, the active material was uniformly mixed with acetylene black and polyvinylidene fluoride (PVDF) at a mass ratio of 8: 1: 1. The mass loading of the active material was approximately 5 mg/cm^2. The electrolyte comprised a 1 M $NaClO_4$ solution in ethylene carbonate (EC)/propylene carbonate (PC) (1: 1 v/v) with a 5% fluoroethylene carbonate (FEC) additive. Cycle and rate performance were recorded using a test system (Neware, MIHW-200-160CH) with a potential range of 2.0–4.2 V (vs. Na^+/Na). Cyclic voltammetry (CV) and electrochemical impedance spectroscopy (EIS) tests were conducted on an electrochemical workstation (Chenhua, CHI604E).

Table S1. Detailed structural information of $NF_{0.5}$VP-CA obtained from XRD Rietveld refinement

Space group=R-3c		R_p=4.49%		R_{wp}=5.73%	
a=8.73087 (Å)		b =8.730873 (Å)		c=21.658480 (Å)	
α =β =90°		γ=120°		V=1429.795 (Å^3)	
Atom	Wyckoff site	X	Y	Z	occ
V	12c	0.000000	0.000000	0.146487	0.750000
Na1	6b	0.000000	0.000000	0.000000	1.000000
Na2	18e	0.630861	0.000000	0.250000	0.833333
P	18e	0.290640	0.000000	0.250000	1.000000
O1	36f	0.191400	0.169020	0.089050	1.000000
O2	36f	0.029000	0.207140	0.193100	1.000000
Fe	12c	0.000000	0.000000	0.146487	0.250000

Table S2. Detailed structural information of $NF_{0.5}$VP-Glc obtained from XRD Rietveld refinement

Space group=R-3c		R_p=4.31%		R_{wp}=5.66%	
a=8.729514 (Å)		b =8.729514 (Å)		c=21.625790 (Å)	
α =β =90°		γ=120°		V=1427.193 (Å^3)	
Atom	Wyckoff site	X	Y	Z	occ
V	12c	0.000000	0.000000	0.146487	0.750000
Na1	6b	0.000000	0.000000	0.000000	1.000000
Na2	18e	0.630861	0.000000	0.250000	0.833333
P	18e	0.290640	0.000000	0.250000	1.000000
O1	36f	0.191400	0.169020	0.089050	1.000000
O2	36f	0.029000	0.207140	0.193100	1.000000
Fe	12c	0.000000	0.000000	0.146487	0.250000

Table S3. Carbon Analysis Report

Sample	Carbon content (wt%)
$NF_{0.5}VP$-CA	4.13
$NF_{0.5}VP$-Glc	5.2

Table S4. The comparison of the performances of recent-studied Fe/V-substituted NASIOCN cathode materials for SIBs.

Sample	Synthetic method	Initial Discharge Capacity	Capacity at High Rate	Carbon content	Reference
$Na_{3.9}FeV_{0.9}Zr_{0.1}(PO_4)_3$	Sol-gel & Calcination	114 mAh g^{-1} at 0.1 C	78.7 mAh g^{-1} at 20C	10.2%	[1]
$Na_3V_{1.94}K_{0.06}(PO_4)_3$	Sol-gel & Calcination	117.3 mAh g^{-1} at 0.5 C	88.3 mAh g^{-1} at 20C	10.1%	[2]
$Na_{3.15}VFe_{0.86}(PO_4)_3$	Sol-gel & Calcination	102.8 mAh g^{-1} at 0.1 C	67.8 mAh g^{-1} at 20C	4.03%	[3]
$Na_4FeV(PO_4)_3$	Ball milling aid Sol-gel & Calcination	99.9 mAh g^{-1} at 0.1 C	80.6 mAh g^{-1} at 10C	6.71%	[4]
$Na_3Fe_{0.8}V_{1.2}(PO_4)_3$	Sol-gel & Calcination	115.2 mAh g^{-1} at 0.1 C	90.4 mAh g^{-1} at 20C	-	[5]
$Na_4FeV_{1/3}Ti_{2/3}(PO_4)_3$	Sol-gel & Calcination	113.5 mAh g^{-1} at 0.5 C	68.2 mAh g^{-1} at 20C	-	[6]
$Na_{3.67}Fe_{0.67}VTi_{0.33}(PO_4)_3$	Sol-gel & Calcination	121.4 mAh g^{-1} at 0.1 C	64.1 mAh g^{-1} at 20C	5.17	[7]
$Na_{3.5}Fe_{0.5}V_{1.5}(PO_4)_3$	**Sand milling aid Spray-dried & Calcination**	**124 mAh g^{-1} at 0.5 C**	**95 mAh g^{-1} at 20 C**	**4.13%**	**This work**

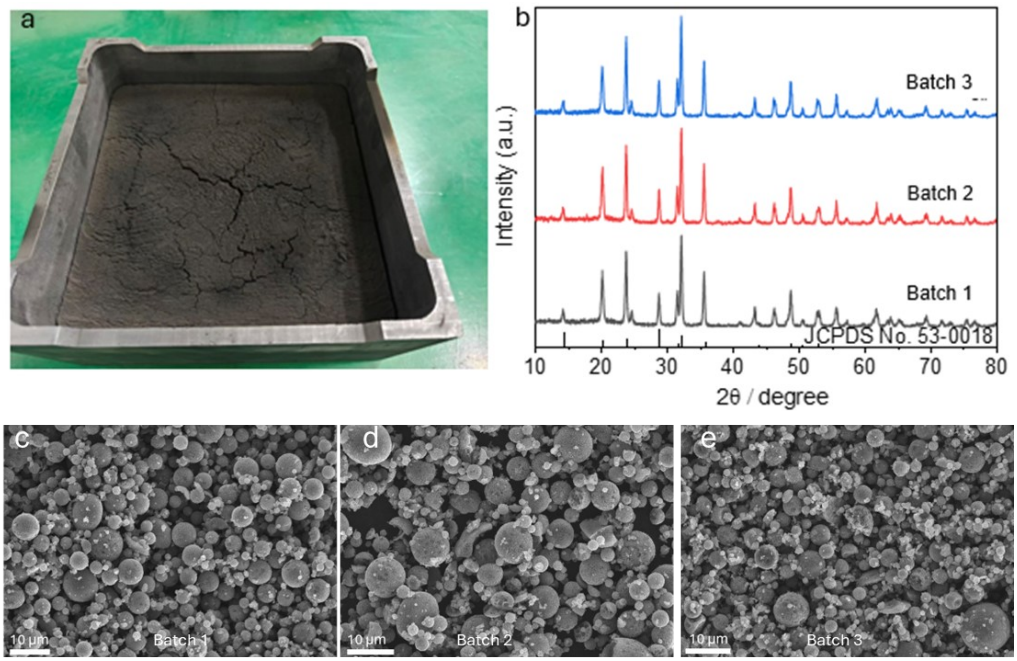

Fig. S1. (a) Photograph, (b) XRD patterns, and SEM images of kilogram-scale NF0.5VP-CA samples from three consecutive batches: (c) Batch 1, (d) Batch 2, and (e) Batch 3.

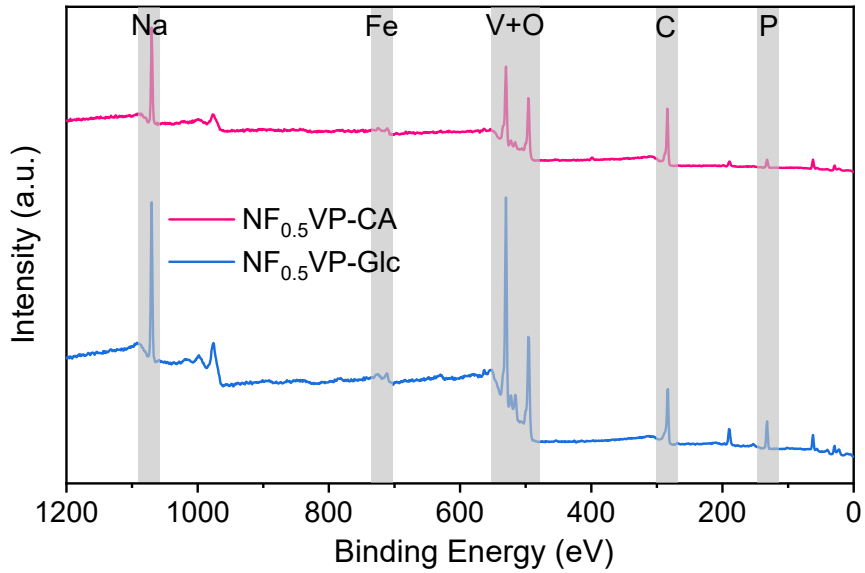

Fig. S2. XPS survey of $NF_{0.5}VP$-CA and $NF_{0.5}VP$-Glc.

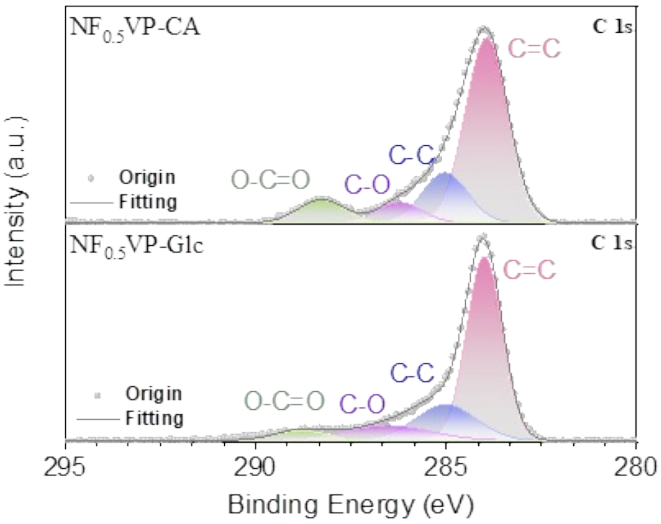

Fig. S3. C 1s XPS of spectra of samples.

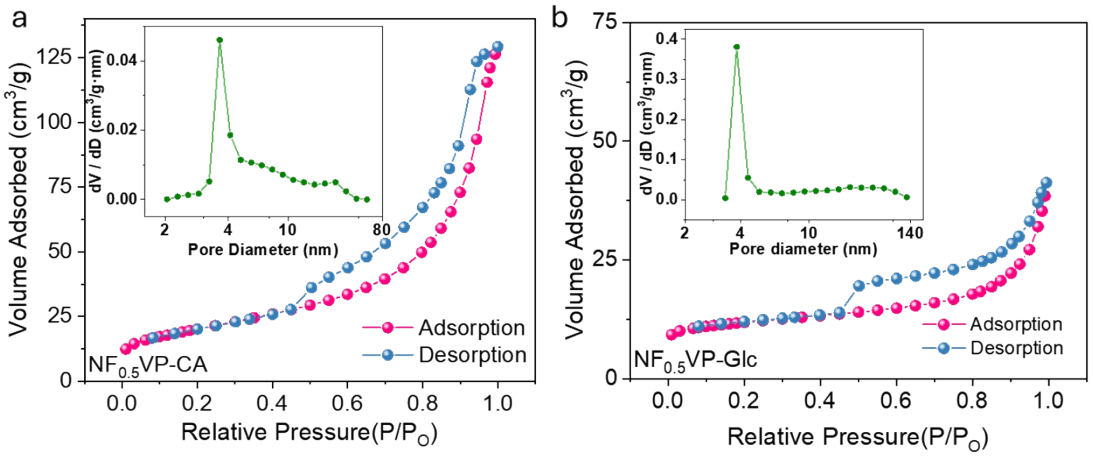

Fig. S4. The nitrogen adsorption–desorption curve with inset pore-size distribution of (a) $NF_{0.5}$VP-CA and (b) $NF_{0.5}$VP-Glc.

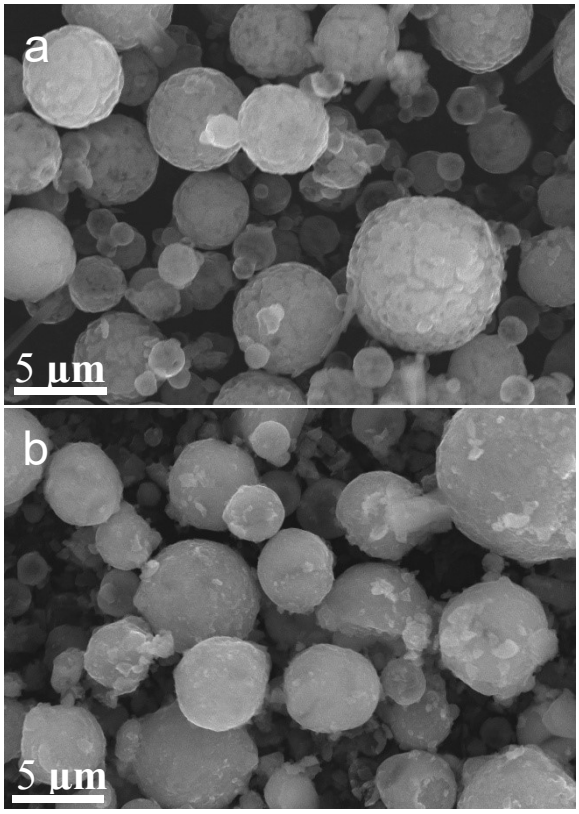

Fig. S5. SEM images of the (a) $NF_{0.5}VP$-CA and (b) $NF_{0.5}VP$-Glc.

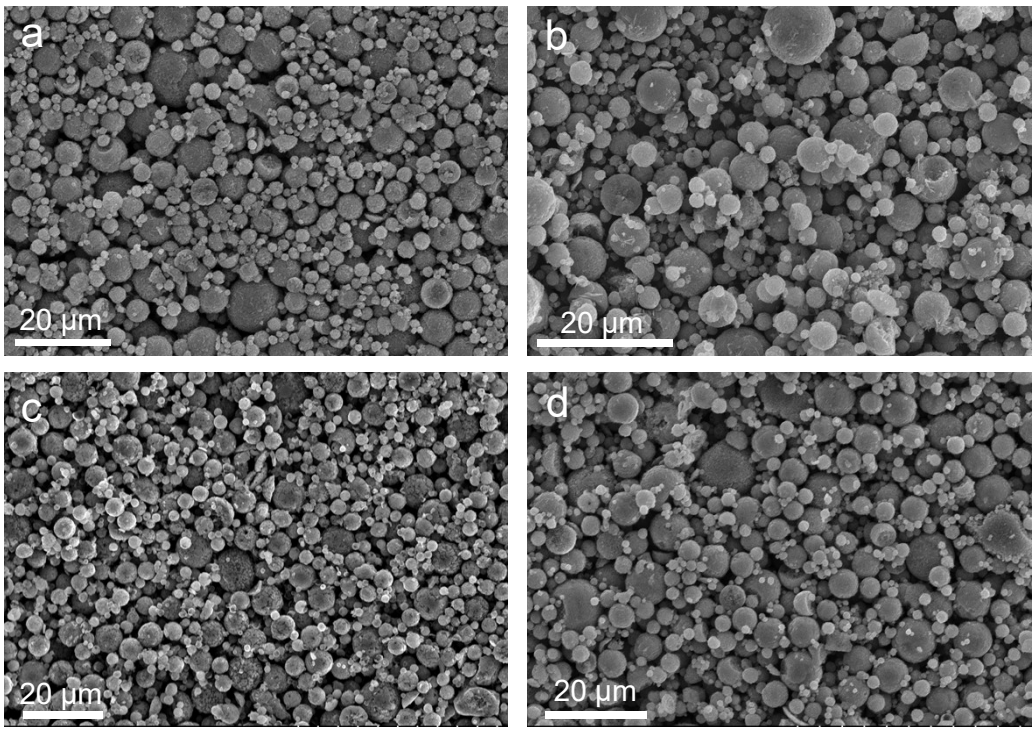

Fig. S6. SEM images of the (a) NVP-CA, (b) $NF_{0.3}VP$-CA, (c) $NF_{0.7}VP$-CA and (d) $NF_{1.0}VP$-CA.

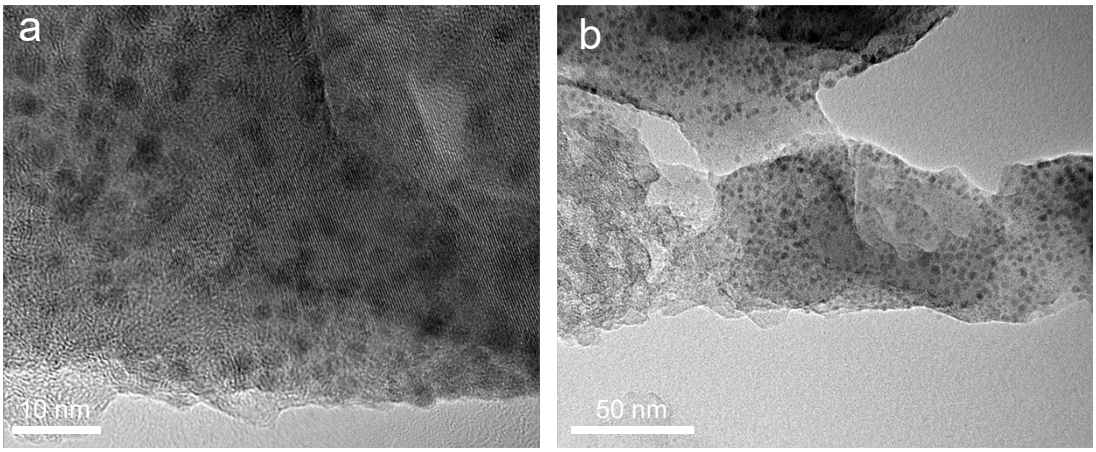

Fig. S7. HR-TEM images (a and b) at different magnifications showing carbon quantum dots (CQDs) uniformly distributed within the carbon coating layer of $NF_{0.5}VP$-CA particles.

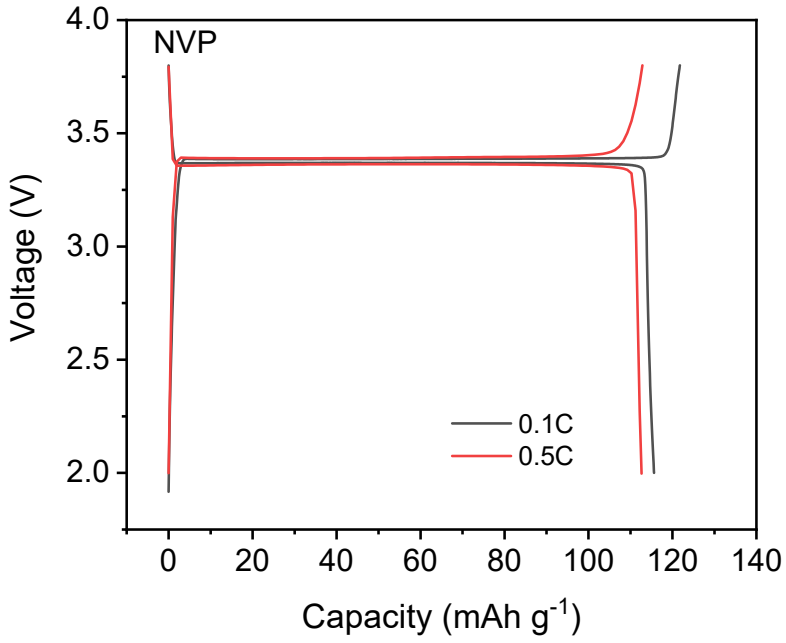

Fig. S8. Charging/discharging performances of NVP range from 2 to 3.8V at 0.1C and 0.5C.

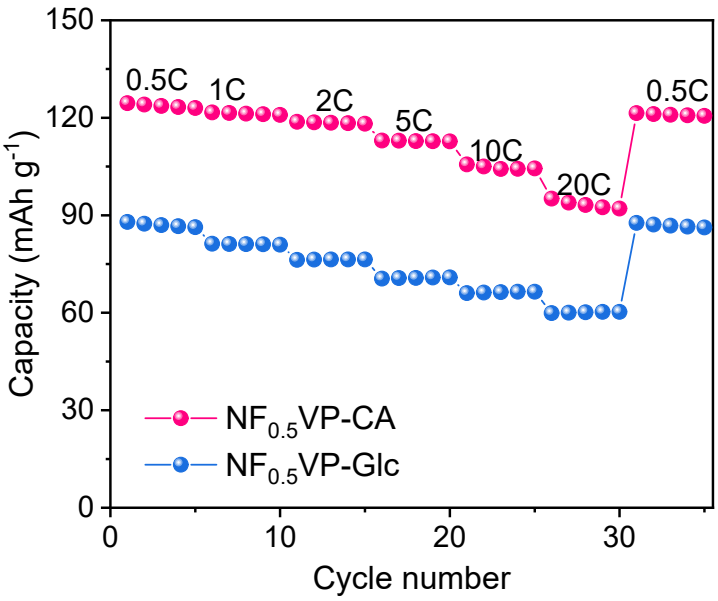

Fig. S9. Rate performance of the $NF_{0.5}VP$-CA and $NF_{0.5}VP$-Glc.

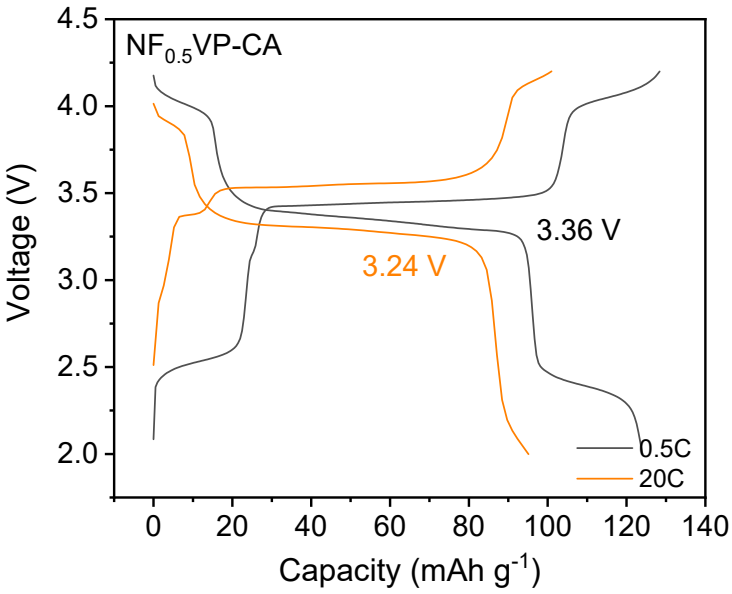

Fig. S10. GCD curves of $NF_{0.5}VP$-CA at 0.5 C and 20 C.

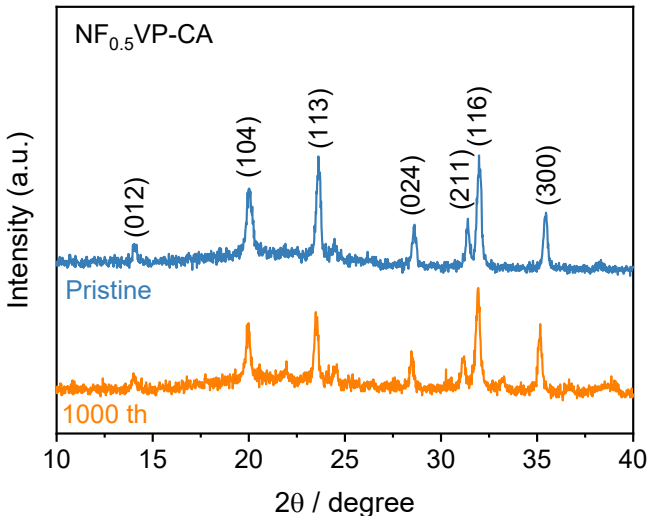

Fig. S11. X-ray diffraction patterns of the $NF_{0.5}$VP-CA electrodes before and after 1000^{th} charge/discharge cycle at the rate of 20 C.

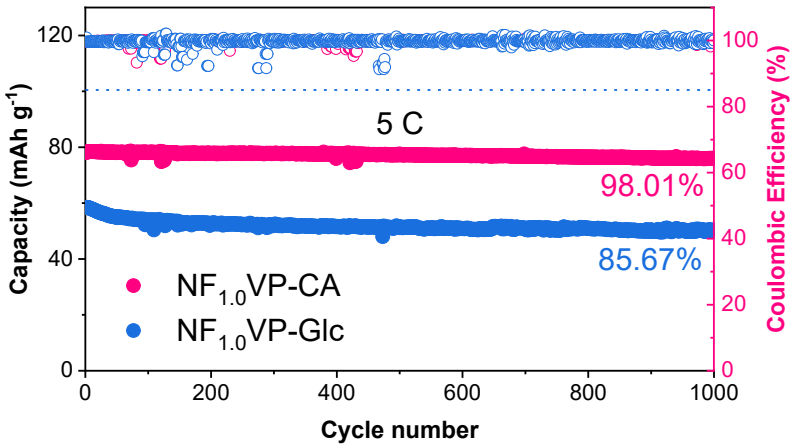

Fig. S12. The long cycling performance comparison for $NF_{1.0}VP$ at 5 C.

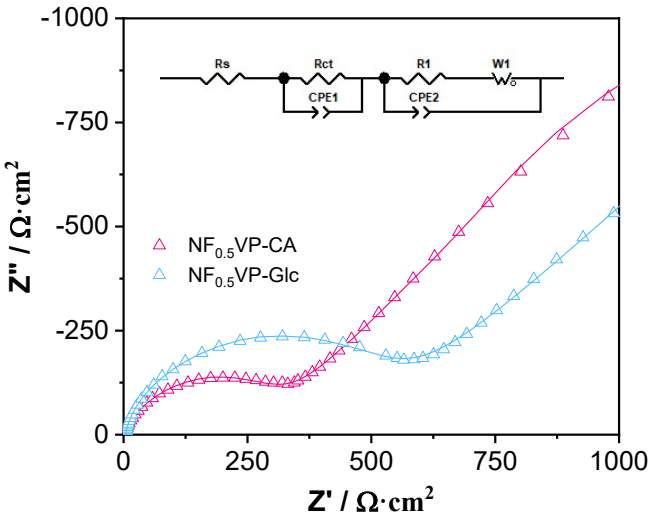

Fig. S13. Electrochemical impedance spectra of $NF_{0.5}VP$-CA and $NF_{0.5}VP$-Glc electrodes.

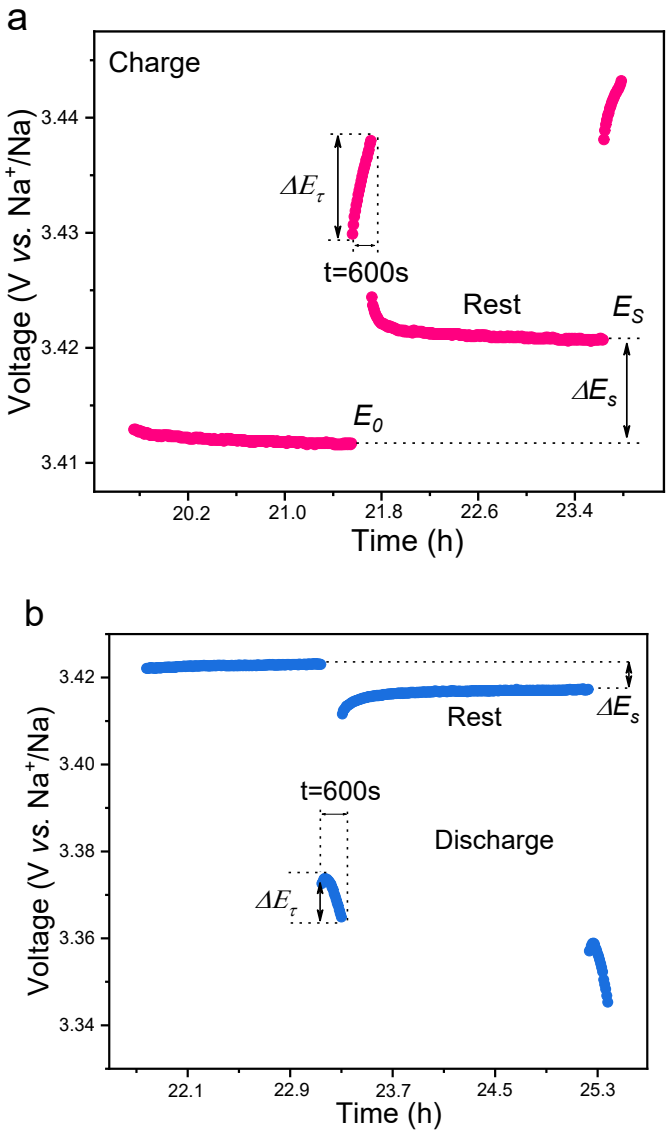

Fig. S14. Schematic diagram of a single GITT titration step around at 3.43 V during the (a) charging process and 3.42 V during the (b)discharging process.

A constant current of 0.2 C lasted for 10 min was carried out on the electrode to control the Na ion insertion and extraction, following by a relaxation process lasting for 120 min. The apparent Na ion diffusion coefficients (D_{Na}) were calculated by the following equation:

$$D^{GITT} = \frac{4}{\pi\tau}\left(\frac{m_b V_m}{M_b S}\right)^2\left(\frac{\Delta E_s}{\Delta E_t}\right)^2, \left(\tau \ll \frac{l^2}{D_{Na}}\right) \quad \text{(Eq. S1)}$$

where D_{Na} is the Na-ion diffusion coefficient in $cm^2\ s^{-1}$. τ is the relaxation time. m_B, M_B, V_m, S represent the mass, molecular weight, molar volume and surface area of the cathode material, respectively. ΔE_s is the difference between two consecutive stable voltages after relaxation, and ΔE_τ is the transient voltage-change during a single titration step.

References:

[1] X. Ma, X. Yu, X. Li, *et at.*, Modulating Na vacancies of $Na_4FeV(PO_4)_3$ via Zr-substitution: Toward a superior rate and ultra stable cathode for sodium-ion batteries, *J. Power Sources*, 2022, 541, 231727.

[2] X. Shen, M. Han, Y. Su, *et at.*, Alkali metal ion induced lattice regulation for all climate NASICON-type cathode with superior Na-storage performance, *Nano Energy*, 2023, 114, 108640.

[3] C. Zhu, X. Liu, C. Li, *et at.*, Sodium-Deficient NASICON $Na_{3+x}VFe(PO_4)_3$ Cathode for High-Performance Sodium-Ion Batteries, *Small Methods*, 2025, 9, 2401697

[4] F. Lu, J. Wang, S. Chang, *et at.*, New-type NASICON-$Na_4FeV(PO_4)_3$ cathode with high retention and durability for sodium ion batteries, *Carbon*, 2022, 196, 562–572.

[5] S. Liu, Z. Xu, L. Ren, *et at.*, Fe-modified NASICON-type $Na_3V_2(PO_4)_3$ as a cathode material for sodium ion batteries, *RSC Adv.*, 2024, 14, 4835–4843.

[6] X. Zhao, X. Wang, Z. Gu, *et at.*, Unlocking Quasi-Monophase Behavior in NASICON Cathode to Drive Fast-Charging Toward Durable Sodium-Ion Batteries, *Adv. Funct. Mater.*, 2024, 34, 2402447.

[7] X. Zhang, Z. Gu, X. Wang, Z. *et at.*, Charge reconfiguration for breaking the V^{4+}/V^{5+} redox barrier in sodium-based NASICON cathode with higher energy density, *Mater. Today*, 2025, 86, 87–95.